Nanoscale

Accepted Manuscript

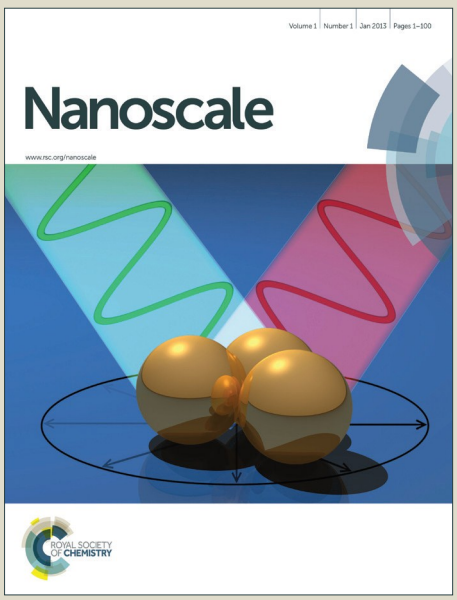

ROYAL SOCIETY OF CHEMISTRY

www.rsc.org/nanoscale

Nanoscale

RSCPublishing

ARTICLE

Optical and Photoacoustic Dual-Modality Imaging Guided Synergistic Photodynamic/Photothermal Therapies

Cite this: DOI: 10.1039/xoxxooooox

Received ooth January 2012,
Accepted ooth January 2012

DOI: 10.1039/xoxxooooox

www.rsc.org/

Xuefeng Yan,[abc] Hao Hu,[b] Jing Lin,[b] Albert J. Jin,[d] Gang Niu,[b] Shaoliang Zhang,[e] Peng Huang,*[b] Baozhong Shen*[ac] and Xiaoyuan Chen*[b]

Phototherapies such as photodynamic therapy (PDT) and photothermal therapy (PTT), due to their specific spatiotemporal selectivity and minimal invasiveness, have been widely investigated as alternative treatments of malignant diseases. Graphene and its derivatives not only have been used as carriers to deliver photosensitizers for PDT, but also as photothermal conversion agents (PTCAs) for PTT. Herein, we strategically designed and produced a novel photo-theranostic platform based on sinoporphyrin sodium (DVDMS) photosensitizer-loaded PEGylated graphene oxide (GO-PEG-DVDMS) for enhanced fluorescence/photoacoustic (PA) dual-modal imaging and combined PDT and PTT. The GO-PEG carrier drastically improves the fluorescence of loaded DVDMS *via* intramolecular charge transfer. Concurrently, DVDMS significantly enhances the near-infrared (NIR) absorption of GO for improved PA imaging and PTT. The cancer theranostic capability of the as-prepared GO-PEG-DVDMS was carefully investigated both *in vitro* and *in vivo*. This novel theranostics is well suited for fluorescence/PA dual-modal imaging and synergistic PDT/PTT.

Introduction

Photodynamic therapy (PDT) is an emerging form of phototherapy using photosensitizers (PSs) that, when exposed to the designated light, can transfer the absorbed photon energy to surrounding oxygen molecules, producing reactive oxygen species (ROS) such as singlet oxygen ($^1O_2$), free radicals, and so on, which can kill cancer cells and destroy tumor tissues[1-8]. However, several issues limit the clinical application of PDT including: i) PSs are prone to photo-bleaching and self-destruction upon prolonged light exposure[9, 10]. ii) PDT involves tissue oxygen consumption, which induces local hypoxia, and eventually ceases the production of $^1O_2$[11]. iii) The limited penetration depth of excitation light (600~700 nm) may also hinder PDT efficacy[12-14]. Recent advances in new synergistic treatment modalities, which combine PDT with other therapies such as photothermal therapy (PTT), hold great promises to overcome those limitations and achieve enhanced therapeutic outcome[15-20].

Several platforms such as gold nanorods[16], gold nanocages[21, 22], gold nanostars[11], gold nanovesicles[7], palladium nanosheets[23], MoS_2 nanosheets[24], and graphene oxide nanosheets[18, 25], have already been used to combine with PSs for synergistic PDT/PTT. For example, we have developed Chlorin e6 (Ce6) functionalized gold nanostars to coordinate PDT with plasmonic PTT upon single continuous wave laser irradiation[11]. Our experimental results demonstrate that the difference in photostability between PSs and gold nanostructures can be used to modulate PDT and PTT by adjusting irradiation time. Although conceptually sound, this method has limitation of relatively low loading capacity of PSs due to the limited surface area of nanostars. Afterwards, we constructed a multifunctional theranostic platform based on Ce6 loaded plasmonic vesicular assembling of gold nanoparticles for tri-modality fluorescence/thermal/photoacoustic (PA) imaging-guided synergistic PTT/PDT with improved efficacy[7]. The loading efficiency was markedly improved because the hollow nature of the assemblies overcomes the limitation of the surface loading. However, the fluorescence of PS is often quenched in these systems, impairing the *in vivo* visualization of pharmacokinetics and treatment efficacy using PS fluorescence imaging. Therefore, the development of novel PS nanocomplexes without fluorescence quenching is highly desirable for optimizing PS fluorescence imaging and synergistic treatment.

In this study, we developed sonoporphyrin sodium (DVDMS), a photosensitizer, loaded PEGylated graphene oxide (GO-PEG-DVDMS) for enhanced fluorescence/PA dual-modal imaging and combined therapies of PDT and PTT (Scheme 1). The DVDMS is a new photosensitizer used for the treatment or diagnosis of cancer, precancerous lesions or benign lesions and shown to have a much higher photoactivity than the clinically used photosensitizer Photofrin[26, 27]. Additionally, DVDMS is water-soluble, stable, of

low skin toxicity, and of high production quality control. We now find that GO-PEG carriers drastically improve the fluorescence of loaded DVDMS *via* intramolecular charge transfer and concurrently DVDMS significantly enhances the near-infrared (NIR) absorption of GO for much improved PA imaging and PTT.

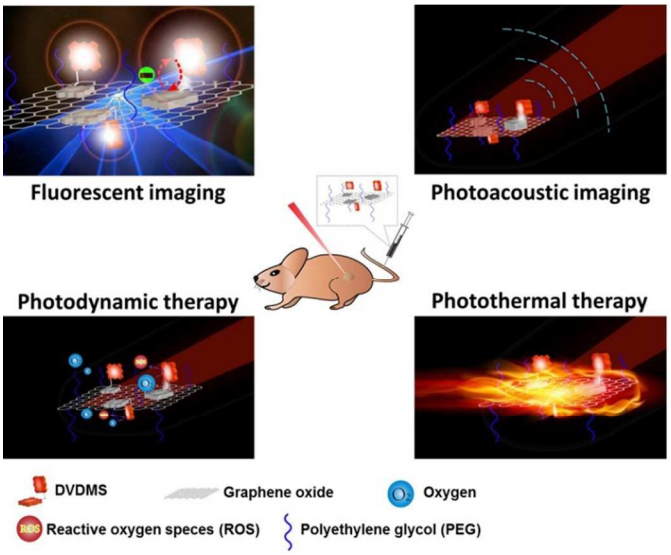

Scheme 1. Schematic illustration of the multi-modality imaging guided synergistic photodynamic/photothermal therapies based on PEG-GO carrier and DVDMS photosensitizer.

Results and Discussion

In the atomic force microscope (AFM) images of GO-PEG and GO-PEG-DVDMS as shown in Fig. 1A, the average diameter of GO-PEG is about 14 nm (with its medium 50% ranging between 7.6 and 16 nm), and the thickness is 1.30 ± 0.55 nm. After DVDMS was loaded, both the average diameter and thickness of GO-PEG-DVDMS increased to about 20.5 nm (with the corresponding medium 50% shifted to between 8.5 and 23 nm) and 1.47 ± 0.82 nm (with an increased population at the height ~ 2 nm), respectively (Fig. 1A).

The absorption spectra of GO-PEG, DVDMS and GO-PEG-DVDMS are shown in Fig. 1B. Pure DVDMS exhibits a strong Soret absorption peak at 385 nm, and Q-bands (500~700 nm). GO-PEG exhibits a peak at 230 nm. After loading of DVDMS by GO-PEG, a new peak appears at 430 nm. It may attribute to the formation of strong π–π stacking interactions between DVDMS and GO-PEG[28-31]. Fig. 1C shows the increased optical absorption intensities at 808 nm with the increase of loaded DVDMS dose, which is propitious to improve the function of PA imaging and PTT of GO-PEG-DVDMS.

Fig. 1D shows the fluorescence spectra of GO-PEG, DVDMS and GO-PEG-DVDMS. No fluorescence signal is observed for GO-PEG. DVDMS shows two fluorescence emission peaks at 618 and 680 nm, respectively. Interestingly, after loading of DVDMS onto GO-PEG, the peaks of GO-PEG-DVDMS are shifted to 644 and 670 nm, respectively. Interestingly, the fluorescence intensity of DVDMS in GO-PEG-DVDMS is dramatically enhanced. In comparison with our previous results[32-34], this phenomenon may be due to the intramolecular energy/charge transfer of GO-PEG-DVDMS[35].

To evaluate the loading efficiency of DVDMS by GO-PEG, the DVDMS was quantified by using the DVDMS UV-vis calibration curve at 516 nm. When the GO-PEG concentration was fixed at 0.1 mg/mL, nearly 51% of DVDMS was loaded onto GO-PEG by incubation with 0.4 mg/mL of DVDMS. This result indicates that GO-PEG can load about 2 times of DVDMS as its weight (Fig. 1E).

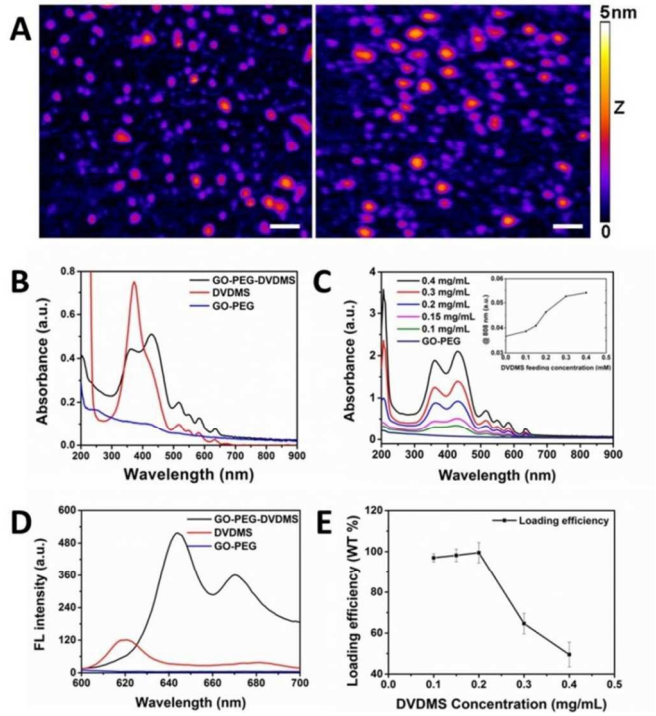

Fig. 1 (A) AFM image of GO-PEG and GO-PEG-DVDMS (white scale bar: 50 nm for X-Y dimension and the height is represented by the 5 nm Z-color bar). (B) UV-vis absorption spectra of GO-PEG (blue), DVDMS (red) and GO-PEG-DVDMS (black). (C) UV-vis absorption spectra of GO-PEG-DVDMS and the optical intensities changes at the wavelength 808 nm with different feeding concentrations of DVDMS (C_{GO-PEG} = 0.1 mg/mL; C_{DVDMS} = 0.1~0.4 mg/mL). (D) The fluorescence spectra of GO-PEG (blue), DVDMS (red) and GO-PEG-DVDMS (black). (E) Drug loading efficiency of GO-PEG-DVDMS in different feeding concentrations of DVDMS (C_{GO-PEG} = 0.1 mg/mL).

The ROS generation of GO-PEG-DVDMS and free DVDMS were compared using SOSG as an indaicator by its fluorescence intensity change at 525 nm[14]. Samples were irradiated with a 630 nm laser and the fluorescence spectra of SOSG were measured at different time points. As shown in Fig. 2A, both free DVDMS and GO-PEG-DVDMS exhibit a sharp increased SOSG fluorescence intensity in a time-dependent manner (Fig. 2B), which suggests that the DVDMS still can generate single oxygen after being loaded by GO-PEG.

To assess the light-to-heat conversion capability of GO-PEG, DVDMS and GO-PEG-DVDMS, the temperature changes of various solutions upon laser irradiation were recorded by an infrared camera (FLIR). As shown in Fig. 2C, the GO-PEG-DVDMS aqueous solution (4 μg/mL of GO-PEG and 8 μg/mL of DVDMS) was exposed to an 808 nm NIR laser at a power density of 1 W/cm^2. GO-PEG (4 μg/mL), DVDMS (8 μg/mL) and water were used as

controls. No obvious temperature change was observed in water control. A slight temperature increase was observed in the DVDMS group. The GO-PEG-DVDMS showed high photothermal conversion effect with a temperature reaching 60.2 °C, which is about 11.1 °C higher than that of GO-PEG (49.1 °C), after 5 min irradiation. These results suggest higher photothermal conversion efficiency of GO-PEG-DVDMS than that of GO-PEG, which can be attributed to the enhanced NIR absorption of GO-PEG by DVDMS. Fig. 2D shows an obvious concentration-dependent temperature increase of GO-PEG-DVDMS upon 808 nm irradiation.

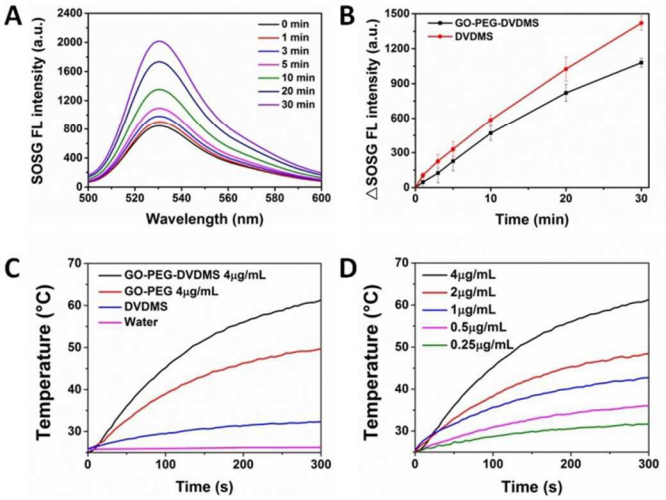

Fig. 2 (A) Fluorescence emission spectra of SOSG (1.0 μM) solution mixed with GO-PEG-DVDMS ($C_{GO\text{-}PEG}$= 0.25 μg/mL, C_{DVDMS}= 0.5 μg/mL) at different laser irradiation time points. (B)The fluorescence intensities change of SOSG's emission peak (525 nm) as a function of laser irradiation times. (GO-PEG-DVDMS: black, DVDMS: red). (C) Temperature change curves of water, DVDMS, GO-PEG, and GO-PEG-DVDMS solutions exposed to the 808 nm laser at a power density of 1 W/cm^2 for 5 min (concentrations of samples are equivalent to 4 μg/mL of GO-PEG or 8μg/mL of DVDMS); (D) Temperature change curves of GO-PEG-DVDMS solutions at different concentrations of GO-PEG ($m_{GO\text{-}PEG}$: m_{DVDMS}=1:2, laser 808 nm, 1 W/cm^2, 5 min).

The dark toxicity of GO-PEG, free DVDMS and GO-PEG-DVDMS in PC9 cells were detected by MTT assay. After 24 h incubation, both free DVDMS and GO-PEG-DVDMS exhibited a concentration-dependent dark toxicity. But at the highest concentration (3 μg/mL of GO-PEG, 6 μg/mL of DVDMS), the cell viabilities were kept above 70.2% (Fig. 3A). Afterwards, the PDT, PTT, and their synergism of GO-PEG-DVDMS were evaluated on the same cell line. For PDT effect, after 24 h incubation, GO-PEG-DVDMS showed better PDT effect than free DVDMS upon same laser irradiation (630 nm, 5 J/well, Fig. 3B). For PTT effect, GO-PEG-DVDMS also showed better PTT effect than either GO-PEG or DVDMS under same laser irradiation (808 nm, 1 W/cm^2, 3 min, Fig. 3C), which is in accordance with the observation in Fig. 2C. The synergistic dual-mode PDT and PTT of GO-PEG-DVDMS were further investigated by the laser irradiation switch from 630 nm laser irradiation (2 J/well) for PDT to 808 nm laser irradiation (1 W/cm^2, 3 min/well) for PTT (Fig. 3D). PDT, PTT, and their synergism effects all show show a concentration-dependent cancer cell killing effect. Compared with either individual PDT or PTT alone, the synergistic therapies of PDT and PTT of GO-PEG-DVDMS exhibited higher therapeutic efficacy. The PDT, PTT, and their synergism effects were also evidenced by live/dead cell staining, which agree with the MTT results (Fig. 3E).

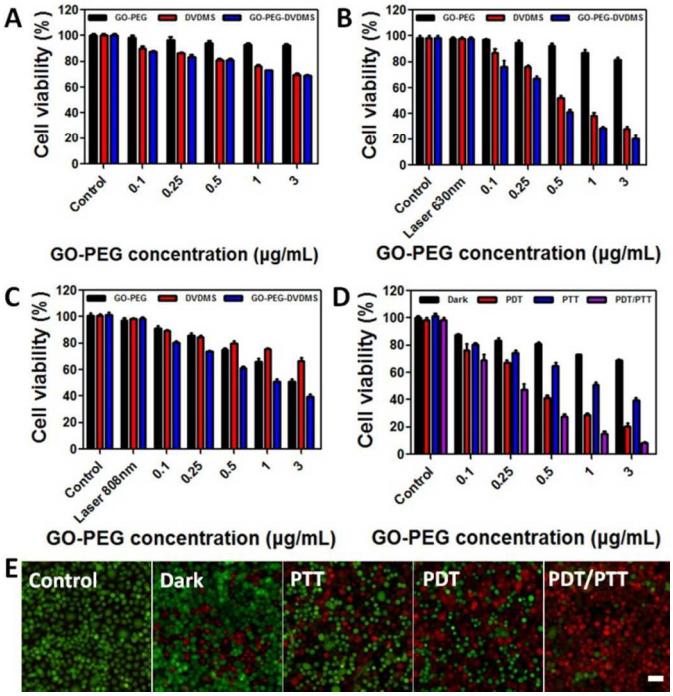

Fig. 3 Relative viabilities of cells incubated with various concentrations of GO-PEG, free DVDMS and GO-PEG-DVDMS ($m_{GO\text{-}PEG}$: m_{DVDMS}=1:2): (A) Dark toxicity (B) PDT effect upon 630 nm laser irradiation (2 J/well). (C) PTT upon 808 nm laser irradiation (1 W/cm^2, 3 min/well). (D) Synergistic effect of PDT and PTT. (E) Fluorescence images of Calcein AM/Ethidium homodimer-1stained PC9 cells incubated with GO-PEG-DVDMS under different treatments (GO-PEG-DVDMS: 1 μg/mL of GO-PEG, 2μg/mL of DVDMS) Scale bars: 100 μm.

For *in vivo* studies, we investigated the tumor accumulation profile of GO-PEG-DVDMS in PC9 tumor-bearing mice using fluorescence and photoacoustic dual-modality imaging. When the tumors reached about 100 mm^3 in volume, the mice were intravenously injected with GO-PEG-DVDMS (1 mg/kg of GO-PEG). At 2 and 4 h post-injection, the GO-PEG-DVDMS fluorescence was broadly distributed over the whole body of the mice. With the increase of blood circulation time, the tumor signal increased along with the whole-body fluorescence signal gradually decreased (Fig. 4A). At 4~24 h post-injection, the tumor tissue can be easily differentiated from the adjacent normal tissue with high contrast, which is due to the high tumor accumulation of GO-PEG-DVDMS.

Additionally, GO-PEG-DVDMS can absorb light and generate a pressure rise by localized thermoelastic expansion, then emit broadband acoustic waves, which can be detected by PA imaging system. To further confirm the tumor accumulation of GO-PEG-DVDMS in PC9 tumor-bearing mice, we performed *in vivo* PA imaging. As shown in Fig. 4B, very weak PA signal was observed in the tumor region before injection. With time, the PA signal of the tumor tissue increased gradually. Region of interest analysis of the PA images also revealed that the signals gradually increased with time. These results indicate that the GO-PEG-DVDMS has a highly

efficient tumor passive targeting ability and long retention time in the tumor tissue.

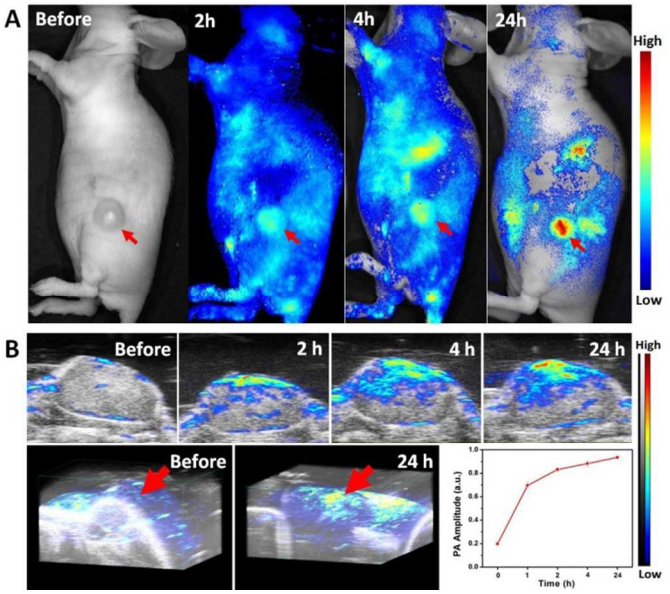

Fig. 4 (A) *In vivo* fluorescence images and (B) Ultrasound/photoacoustic images and quantitative analysis of PA signal of PC9 bearing mice treated with GO-PEG-DVDMS (GO-PEG 1 mg/kg, DVDMS 2 mg/kg) at 2, 4 and 24 h post-injection.

For *in vivo* PTT study, PC9 tumor-bearing mice were intravenously injected with 200 μL of GO-PEG-DVDMS at 0.25 mg/mL (a dose of 2.5 mg/kg of GO-PEG). According to the dual-modality imaging results, 24 h post-injection of GO-PEG-DVDMS was the most suitable time to implement treatment. The PTT treatment was conducted by 808 nm laser irradiation at a power density of 1 W/cm^2 for 10 min. As shown in Fig. 5A, the temperature of tumors in mice treated with GO-PEG-DVDMS increased to 57 °C within 10 min upon laser irradiation, while that in saline group reached only to 32 °C. The temperature of tumor tissues increased by 7 to 29 °C within 10 min under different laser power (0.25~1 W/cm^2) (Fig. 5B). The 3D temperature distribution indicated no significant temperature rise in other body parts of the mice (Fig. 5C). All tumors treated with GO-PEG-DVDMS and laser irradiation were effectively ablated, leaving black scars at the original tumor sites, which were fully recovered about 1 week after treatment (Fig. 6A). In contrast, the tumors in the control groups all grew at similar speed, which suggested that neither laser irradiation nor GO-PEG-DVDMS without laser irradiation inhibited tumor growth (Fig. 6B). No obvious sign of toxicity, such as significant body weight drop, was noticed during this period of observation (Fig. 6C).

From the PTT treatment results, the injection dose of GO-PEG-DVDMS is as high as 2.5 mg/kg of GO-PEG and 5 mg/kg of DVDMS. Synergistic PDT/PTT may have high therapeutic efficacy at low injection dose of GO-PEG-DVDMS. Afterwards, the injection dose of GO-PEG-DVDMS was decreased to 1.0 mg/kg of GO-PEG and 2.0 mg/kg of DVDMS. After 24 h post-injection, tumor tissues were irradiated with a 630 nm laser to induce PDT effect. Then the 808 nm laser irradiation was used for PTT treatment. Both 630 and 808 nm laser spots were adjusted to cover the whole tumor. As shown in 7A & B, the temperature of tumors reached to nearly 47 °C. No significant temperature rise was observed in saline group.

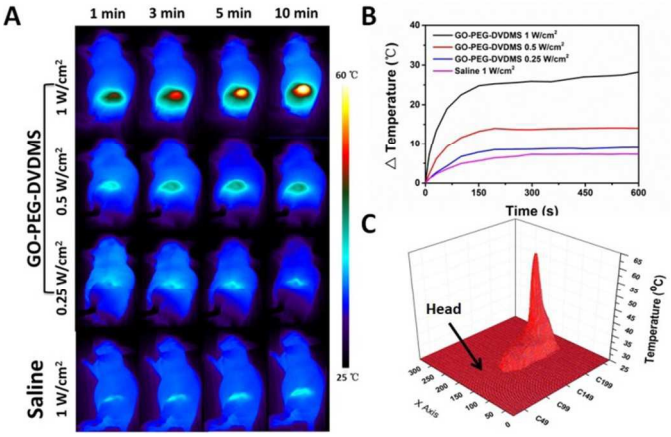

Fig. 5 (A) Infrared thermographic maps of mice under different conditions (2.5 mg/kg of GO-PEG, 5 mg/kg of DVDMS, 808 nm laser). (B) *In vivo* photothermal effect of GO-PEG-DVDMS in tumor region at various concentrations. (C) 3D temperature map of mouse under 808 nm laser irradiation.

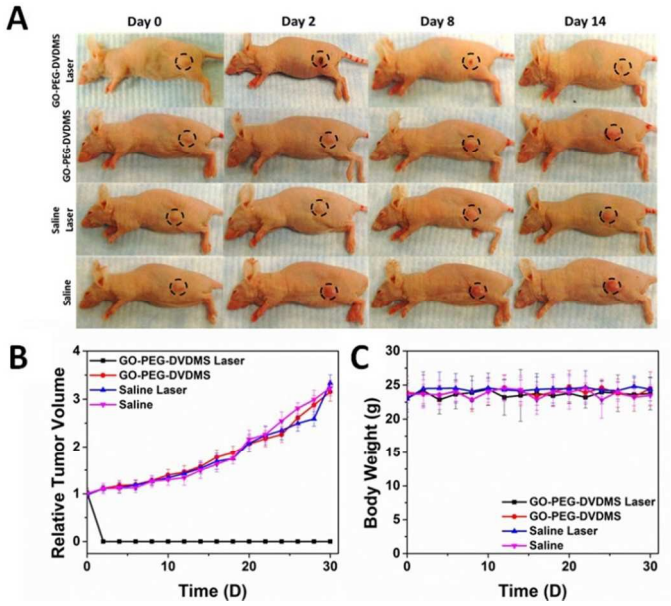

Fig. 6 (A) Representative photos of PC9 tumor-bearing mice before and after PTT treatment from different groups. (B) Tumor growth curves of different groups of tumor-bearing mice after treatment. (C) Body weight curves of PC9 tumor bearing mice after treatment.

Obviously, PDT only treated mice showed significant decrease in tumor growth as compared to the saline-treated mice whereas PTT only treatment showed a slight reduction in tumor growth rate and tumors started to regrow after day 4 (Fig. 7D). It is worth noting that the GO-PEG-DVDMS group (1 mg/kg of GO-PEG) exhibited significantly higher therapeutic efficacy compared with either individual PDT or PTT alone. No tumor relapse was observed in any of the mice treated with PDT followed by PTT dual-mode therapies, showing complete regression of tumor. Compared with the control group, the PDT and PTT only showed 76% and 34% inhibition,

respectively. (Fig. 7C, D). Complete tumor regression was realized by intravenous injection of GO-PEG-DVDMS, at low injection dose of 1 mg/kg of GO-PEG and 2 mg/kg of DVDMS. All treated mice without weight loss were observed during the treatment (Fig. 7E).

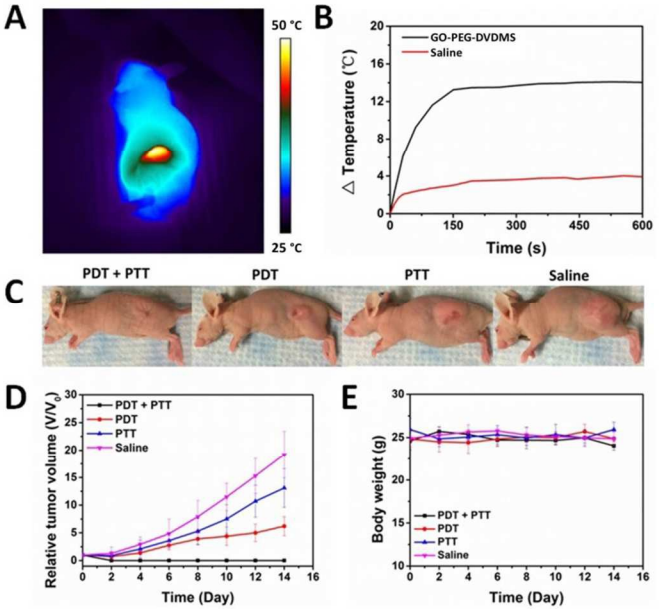

Fig. 7 *In vivo* synergistic therapies of GO-PEG-DVDMS. (A) Infrared thermographic maps of mice injected with GO-PEG-DVDMS upon 808 nm laser irradiation (1 mg/kg of GO-PEG, 2 mg/kg of DVDMS; laser 1 W/cm^2, 10 min). (B) Temperature change curves of tumor tissues of mice treated with GO-PEG-DVDMS or PBS upon same laser irradiation. (C) Representative photos of PC9 tumor-bearing mice from different group after treatment of PDT, PTT or their synergism on day 14. (D) Tumor growth curves of different groups of tumor-bearing mice after different treatments. (E) Body weight curves of PC9 tumor mice after different treatments.

Experimental Section

Synthesis of GO-PEG-DVDMS

PEGylated GO was synthesizedas previously reported[30, 31, 36]. The GO-PEG concentration was recorded with a weight extinction coefficient 47.6 mg mL^{-1}cm^{-1} by using the absorbance at 230 nm. DVDMS aqueous solutions (0.1~0.4 mg/mL) were added into GO-PEG (0.1 mg/mL) aqueous solution. The mixtures were incubated overnight to produce GO-PEG-DVDMS. Free DVDMS was washed by filtration through a 100 kDa cutoff spin filter with distilled deionized (DD) water for 6~8 times.

Characterization of GO-PEG-DVDMS

The size and thickness of GO-PEG-DVDMS was estimated by atomic force microscopic (AFM) images. The Ultraviolet-visible (UV-vis) absorbance spectra were measured to determine the concentration of loaded DVDMS. The optical intensities of GO-PEG-DVDMS at 516 nm were subtracted the part contributed by GO-PEG, and then the concentrations of DVDMS were calculated by a molar extinction coefficient of 2.9 × 10^4 M^{-1}cm^{-1}. Fluorescence spectra of samples were measured by an F-7000 fluorescence spectrophotometer (Hitachi, Tokyo, Japan).

Singlet oxygen generation

To detect the singlet oxygen generation by GO-PEG-DVDMS, Singlet oxygen sensor green (SOSG) was used as an indicator [26]. Briefly, SOSG was dissolved in water containing 2% methanol at a final concentration of 1.0 μM. The DVDMS or GO-PEG-DVDMS was added to the SOSG solution. Each sample was then irradiated with a 630 nm laser (Reserch Electro-Optics Inc, Colorado, US). After irradiated for specific time, SOSG fluorescence emission was measured with an F-7000 fluorescence spectrophotometer (Hitachi, Tokyo, Japan). The SOSG fluorescence enhancement was compared with control sample.

Photothermal effect measurement

To investigate the photothermal efficiency of GO-PEG-DVDMS under the NIR laser irradiation, 200 μL solutions containing different materials were irradiated by a NIR laser (808 nm) for 5 min under different laser densities which were calibrated and measured by a LPE-18 laser power/energy meter. The temperatures of the solutions were monitored by an IR thermal imaging system.

In vitro cytotoxicity and effects of PDT/PTT

The PC9 cells were grown in 96-well plates (8 × 10^3 cells per well) for overnight. Equimolar DVDMS as free DVDMS or GO-PEG-DVDMS were added into the wells and incubated at 37 °C for 24 h in the dark. For toxicity study, after 24 h incubation, cells were washed three times with PBS and 10 μL of MTT solution (5 mg/mL MTT in PBS, pH 7.4) was added into each well and incubated for another 4 h. Then the cells were washed by PBS. Afterwards, 100 μL of DMSO was added per well. Till the intracellular formazan crystals were fully dissolved, the absorbance of 490 nm was recorded using a plate reader. The cell viability was caculated using untreated group as control. On the other hand, before photo treatment, the medium was replaced with fresh drug-free medium, which were immediately irradiated by laser (PDT: 630 nm, 5 J/well; PTT: 808 nm, 1 W/cm^2, 5 min). After irradiation, the cells were kept for another 24 h. Cell viability was estimated by the standard MTT assay.

Tumor models

Athymic nude mice, aged 6-8 weeks, were obtained from Harlan laboratories (Frederick, USA) under protocols approved by the National Institutes of Health Clinical center Animal Care and Use Committee (NIH CC/ACUCC). The PC9 tumor models were injected of 5×10^6 (for PTT study) or 1×10^7 (for combined therapy study) by subcutaneous cells in 100 μL PBS into the left flank of nude mice.

In vivo imaging of GO-PEG-DVDMS

Mice bearing PC9 xenografted tumors (n=3) were anesthetized by inhalation of isoflurane (2 % in 100 % oxygen). The mice were intravenously injected with GO-PEG-DVDMS (1 mg/kg of GO-PEG, 2 mg/kg of DVDMS). Then the mice were imaging using Maestro II optical imaging system (Caliper Life Sciences, Hopkinton, MA) at 2, 4 and 24 h post-injection. The PA imaging of tumor tissues was recorded on a PA imaging system (Vevo 2100, Visual Sonics, Inc.) equipped with a 40 MHz array linear transducer with 256 elements.

***In vivo* therapy study**

Because PTT is dependent on both drug dose and laser power, we tried first to find a best available condition. Tumor bearing mice were injected with 2.5 mg/kg or 1 mg/kg of GO-PEG through tail vein. Then tumors were irradiated by 10 min of 808 nm laser irradiation (1, 0.5 or 0.25 W/cm^2) at 24 h post-injection while the real-time temperature change of tumor surface was monitored by an IR thermal imaging system.

For the study of combined treatment, mice bearing PC9 tumor were randomized into 4 groups (n=5) after following treatment: (a) PDT+PTT group; (b) PDT group; (c) PTT group; (d) control group, when the tumors reached a size around 100 mm^3. For therapeutic treatment, the mice of control group were received only saline solution whereas mice of the other groups were received GO-PEG-DVDMS with dose 1 mg/kg of GO-PEG by tail vein injection. The tumors were subjected to various photoirradiation treatments at 24 h post-injection, including PDT treatment (630 nm, 50 J) only, PTT treatment (808 nm, 1.0 W/cm^2, 10 min) only and forward or reverse sequence of initial PDT and subsequent PTT treatment (PDT/PTT or PTT/PDT). The tumor growth was calculated over 14 days after treatment. Tumor size was monitored with a digital caliper every other day and tumor volume was calculated as follows: $V = LW^2/2$, where L is measured at the longest point and W is at the widest point. Relative tumor volumes were normalized against the original volumes at 0 day for monitoring the tumor growth. The body weights of all mice were measured twice a week.

Conclusions

In summary, we successfully developed a novel photo-theranostic platform based on DVDMS loaded PEGylated GO for both cancer imaging and treatment. The GO-PEG carrier can drastically improve the fluorescence of loaded DVDMS *via* intramolecular charge transfer. Concurrently, DVDMS can enhance the NIR absorption of GO for improved PA imaging and PTT. Meanwhile, GO-PEG carrier can improve tumor accumulation efficiency of DVDMS by enhanced permeability and retention (EPR) effect. GO-PEG-DVDMS exhibit significantly higher therapeutic efficacy compared with either individual PDT or PTT alone. 100% *in vivo* tumor elimination is achieved by intravenous injection of GO-PEG-DVDMS, at low injection dose of 1 mg/kg of GO-PEG and 2 mg/kg of DVDMS. Our strategy provides a single GO-PEG-DVDMS platform for fluorescence/PA dual-modal imaging guided synergistic PDT/PTT, with a great potential for new generation cancer theranostics.

Acknowledgements

This work was supported, in part, by the National Basic Research Program of China (2013CB733802, 2014CB744503, 2015CB931800 and 2015CB931803), National Natural Science Foundation of China (81371596, 81401465, 81130028, 31210103913), the Key Grant Project of Heilongjiang Province (GA12C302), the Ph.D. Programs Foundation of Ministry of Education of China (201123071100203), the Key Laboratory of Molecular Imaging Foundation(College of Heilongjiang Province) and by the intramural research program of the National Institute of Biomedical Imaging and Bioengineering (NIBIB), National Institutes of Health (NIH).

Notes

[a]*Department of Radiology, the Fourth Hospital of Harbin Medical University, Harbin, Heilongjiang, China*
[b]*National Institute of Biomedical Imaging and Bioengineering (NIBIB), National Institutes of Health (NIH), 31 Center Drive, Bethesda, Maryland 20892, United States*
[c]*Molecular Imaging Center of Harbin Medical University, Harbin, Heilongjiang, China*
[d]*Laboratory of Cellular Imaging and Macromolecular Biophysics, National Institute of Biomedical Imaging and Bioengineering (NIBIB), National Institutes of Health, Bethesda, Maryland 20892, United States*
[e]*Jiangxi Qinglong Group Co., Ltd, No. 283 Dongfeng Street, Yichun, Jiangxi 336000, China*

* Corresponding authors: peng.huang@nih.gov (Peng Huang); shenbzh@vip.sina.com (Baozhong Shen); shawn.chen@nih.gov (Xiaoyuan Chen)

Reference

1 Z. Zhang, J. Wang and C. Chen, *Adv. Mater.*, 2013, **25**, 3869-3880.
2 P. Huang, J. Lin, S. Wang, Z. Zhou, Z. Li, Z. Wang, C. Zhang, X. Yue, G. Niu, M. Yang, D. Cui and X. Chen, *Biomaterials*, 2013, **34**, 4643-4654.
3 J. F. Lovell, C. S. Jin, E. Huynh, H. Jin, C. Kim, J. L. Rubinstein, W. C. Chan, W. Cao, L. V. Wang and G. Zheng, *Nat. Mater.*, 2011, **10**, 324-332.
4 Z. Zhang, J. Wang and C. Chen, *Theranostics*, 2013, **3**, 223-238.
5 T. J. Dougherty, C. J. Gomer, B. W. Henderson, G. Jori, D. Kessel, M. Korbelik, J. Moan and Q. Peng, *J. Natl. Cancer I.*, 1998, **90**, 889-905.
6 J. Chen, L. Keltner, J. Christophersen, F. Zheng, M. Krouse, A. Singhal and S. S. Wang, *Cancer J.*, 2002, **8**, 154-163.
7 J. Lin, S. Wang, P. Huang, Z. Wang, S. Chen, G. Niu, W. Li, J. He, D. Cui, G. Lu, X. Chen and Z. Nie, *ACS Nano*, 2013, **7**, 5320-5329.
8 P. Huang, Z. Li, J. Lin, D. Yang, G. Gao, C. Xu, L. Bao, C. Zhang, K. Wang, H. Song, H. Hu and D. Cui, *Biomaterials*, 2011, **32**, 3447-3458.
9 P. Rai, S. Mallidi, X. Zheng, R. Rahmanzadeh, Y. Mir, S. Elrington, A. Khurshid and T. Hasan, *Adv. Drug Deliver. Rev.*, 2010, **62**, 1094-1124.
10 J. F. Lovell, T. W. Liu, J. Chen and G. Zheng, *Chem. Rev.*, 2010, **110**, 2839-2857.
11 S. Wang, P. Huang, L. Nie, R. Xing, D. Liu, Z. Wang, J. Lin, S. Chen, G. Niu, G. Lu and X. Chen, *Adv. Mater.*, 2013, **25**, 3055-3061.
12 D. K. Chatterjee, L. S. Fong and Y. Zhang, *Adv. Drug Deliver. Rev.*, 2008, **60**, 1627-1637.
13 A. P. Castano, T. N. Demidova and M. R. Hamblin, *Photodiagn. Photodyn.*, 2004, **1**, 279-293.
14 P. Huang, J. Lin, X. Wang, Z. Wang, C. Zhang, M. He, K. Wang, F. Chen, Z. Li, G. Shen, D. Cui and X. Chen, *Adv. Mater.*, 2012, **24**, 5104-5110.
15 R. Chen, X. Wang, X. Yao, X. Zheng, J. Wang and X. Jiang, *Biomaterials*, 2013, **34**, 8314-8322.

16 B. Jang, J. Y. Park, C. H. Tung, I. H. Kim and Y. Choi, *ACS Nano*, 2011, **5**, 1086-1094.
17 J. Wang, G. Zhu, M. You, E. Song, M. I. Shukoor, K. Zhang, M. B. Altman, Y. Chen, Z. Zhu, C. Z. Huang and W. Tan, *ACS Nano*, 2012, **6**, 5070-5077.
18 A. Sahu, W. I. Choi, J. H. Lee and G. Tae, *Biomaterials*, 2013, **34**, 6239-6248.
19 Y. Wang, H. Wang, D. Liu, S. Song, X. Wang and H. Zhang, *Biomaterials*, 2013, **34**, 7715-7724.
20 M. Guo, H. Mao, Y. Li, A. Zhu, H. He, H. Yang, Y. Wang, X. Tian, C. Ge, Q. Peng, X. Wang, X. Yang, X. Chen, G. Liu and H. Chen, *Biomaterials*, 2014, **35**, 4656-4666.
21 L. Gao, J. Fei, J. Zhao, H. Li, Y. Cui and J. Li, *ACS Nano*, 2012, **6**, 8030-8040.
22 A. Srivatsan, S. V. Jenkins, M. Jeon, Z. Wu, C. Kim, J. Chen and R. K. Pandey, *Theranostics*, 2014, **4**, 163-174.
23 Z. Zhao, S. Shi, Y. Huang, S. Tang and X. Chen, *ACS Appl. Mater. Inter.*, 2014, **6**, 8878-8885.
24 T. Liu, C. Wang, W. Cui, H. Gong, C. Liang, X. Shi, Z. Li, B. Sun and Z. Liu, *Nanoscale*, 2014, **6**, 11219-11225.
25 B. Tian, C. Wang, S. Zhang, L. Feng and Z. Liu, *ACS Nano*, 2011, **5**, 7000-7009.
26 F. Li, S.-J. Park, D. Ling, W. Park, J. Y. Han, K. Na and K. Char, *J. Mater. Chem. B*, 2013, **1**, 1678.
27 J. Hu, X. Wang, K. Zhang, P. Wang, X. Su, Y. Li, Z. Huang and Q. Liu, *Anticancer Drugs*, 2014, **25**, 174-182.
28 K. Yang, S. Zhang, G. Zhang, X. Sun, S. T. Lee and Z. Liu, *Nano Lett.*, 2010, **10**, 3318-3323.
29 X. Sun, Z. Liu, K. Welsher, J. T. Robinson, A. Goodwin, S. Zaric and H. Dai, *Nano Res.*, 2008, **1**, 203-212.
30 K. Yang, L. Feng, H. Hong, W. Cai and Z. Liu, *Nat. Protoc.*, 2013, **8**, 2392-2403.
31 Z. Sun, P. Huang, G. Tong, J. Lin, A. Jin, P. Rong, L. Zhu, L. Nie, G. Niu and F. Cao, *Nanoscale*, 2013, **5**, 6857-6866.
32 P. Huang, S. Wang, X. Wang, G. Shen, J. Lin, Z. Wang, S. Guo, D. Cui, M. Yang and X. Chen, *J. Biomed. Nanotechnol.*, 2015, **11**, 117-125.
33 P. Rong, K. Yang, A. Srivastan, D. O. Kiesewetter, X. Yue, F. Wang, L. Nie, A. Bhirde, Z. Wang, Z. Liu, G. Niu, W. Wang and X. Chen, *Theranostics*, 2014, **4**, 229-239.
34 P. Huang, C. Xu, J. Lin, C. Wang, X. Wang, C. Zhang, X. Zhou, S. Guo and D. Cui, *Theranostics*, 2011, **1**, 240-250.
35 J. Geng, L. Zhou and B. Liu, *Chem. Commun. (Camb)*, 2013, **49**, 4818-4820.
36 W. S. Hummers Jr and R. E. Offeman, *J. Am. Chem. Soc.*, 1958, **80**, 1339-1339.